Thermal Stability of an Al-Mg-Si alloy after Equal Channel Angular Pressing

T Khelfa, R Lachhab, H Azzeddine, F Li, J A Muñoz-Bolaños, J M Cabrera-Marrero, T Baudin, A L Helbert, F Brisset, M Khitouni

Thermal Stability of an Al-Mg-Si alloy after Equal Channel Angular Pressing

T. Khelfa[1,2*¶], R. Lachhab[2¶], H. Azzeddine[3], F. Li[1], J. A. Muñoz-Bolaños[4], J. M. Cabrera-Marrero[5,6], T. Baudin[7], A. L Helbert[7], F. Brisset[7], M. Khitouni[2]

[1]*State Key Laboratory of Solidification Processing, School of Materials Science and Engineering, Northwestern Polytechnical University, Xi'an 710072, China*

[2]*Laboratory of Inorganic Chemistry Ur-11-ES-73, Faculty of Sciences, University of Sfax, 1171, 3018-Sfax, Tunisia.*

[3]*Department of Physics, University of Mohamed Boudiaf, M'sila, 28000, Algeria*

[4]*National University of Science and Technology "MISIS", Moscow 119049, Russia*

[5]*Department of Materials Science and Metallurgical Engineering, Universitat Politècnica de Catalunya, EEBE-c/Eduard Maristany 10-14, 08019- Barcelona, Spain*

[6]*Institute of Research in Metallurgyc and Materials, Universidad Michoacana de San Nicolás de Hidalgo, Edificio "U-3", Ciudad Universitaria, 58030-Morelia, Michoacán, México*

[7]*Université Paris-Saclay, CNRS, Institut de chimie moléculaire et des matériaux d'Orsay, 91405 Orsay, France*

Abstract

AA6060 aluminum alloy was subjected to severe plastic deformation (SPD) through Equal Channel Angular Pressing (ECAP) up to 8 passes *via* route B_C. ECAPed samples isochronally annealed for 1 hour at a temperature range of 150- 450°C. The microstructure and texture of the studied material were evaluated by Electron Back scatter Diffraction (EBSD), and the microhardness was characterized by Vickers microhardness testing. It was found that shearing texture is typically enhanced after ECAP processing. Grain size and grain growth kinetics were also studied. ECAP led to a substantial rise in hardness, with stability following 4 passes. Microstructures and material properties were relatively stable up to annealing temperatures of 150 °C. Some sub-micrometer grains were kept in the 8 passes sample to annealing temperatures of 300 °C. Annealing at elevated temperature resulted in a reduction in hardness leading to a rise in grain size and a decrease in dislocation density. After annealing temperature up to 450 °C, the texture index reveals a tendency to the texture weakening and

randomization. The activation energy required for the grain growth of the AA6060 alloy was exceptionally low above 300°C.

Keywords: Aluminum alloy, ECAP; Microstructure; Texture; Hardness; Activation energy

* Corresponding author: tarekkhelfa@nwpu.edu.cn

¶ These authors contributed equally to this work.

1. Introduction

Severe plastic deformation (SPD) is perhaps one of the most promising techniques to create ultra-fine grained (UFG) materials [1-3]. Equal-channel angular pressing (ECAP) as among the most efficient and attainable processes of severe plastic deformation (SPD) has extensive applications thanks to the manufacture of nanostructured (NS) and UFG metals and alloys [4,5]. On the other hand, it is well established that using SPD processes, the physical and mechanical properties of metallic materials can be significantly improved [6]. Additionally, SPD processes may also cause important changes in the evolution of microstructure and crystallographic texture relative to traditional processing methods [7].

AA6000 series aluminum alloys have drawn interest in the aviation, automotive, electrical engineering, and building industries thanks to their lightweight, excellent strength, high conductivity, and reasonable corrosion properties [8-11]. Several studies have concentrated on the evaluation of AA6000 series alloys after ECAP processing [12-15]. For example in [15], AA6060 samples were severely ECAPed at ambient temperature up to 12 ECAP passes *via* route B_C. In overall behavior, samples exhibited an equiaxed array of UFG microstructure and a rapid increase in high-angle grain boundaries (HAGB) fraction after 5 passes while a greater number of passes demonstrate a limited effect on strength and no significant change in the average grain size. In spite of the fact that UFG alloys can have remarkable mechanical properties, they can not be utilized at high temperatures except the microstructures are steady. In fact, the annealing temperature can strongly affect the microstructure evolution which has a significant impact on the physical, chemical, and mechanical characteristics.

Then, developing a better comprehension of the thermal stability behavior of UFG structures produced by ECAP claims interest from the scientific community. Recently, extensive research work has been performed to examine the impact of annealing on microstructure development of highly deformed materials (Cu, Al, Fe, Mg) [16-20] and Al alloys [21-24]. It was reported by Liang et al. [16] that a lower number of ECAP passes results in retarded recrystallization process to longer annealing duration or elevated annealing temperature. With approximately the same strength properties and improved thermal stability, the microstructure got after 2 ECAP passes has some benefit in terms of the cost of production as opposed to 16 ECAP passes. Studying the annealing behavior of Al-0.13% and Mg Al-3%Mg treated by the ECAP process, Prangnell et al. [24] mentioned that the early stages of annealing were considered to be particularly susceptible to the misorientation and distribution of the low angle boundaries maintained inside the structure of deformation. According to Dhal et al. [23], after annealing treatment, the precipitation of Cu_2Al and AlCuMgSi particles in UFG Al 2014 alloy resulted in better thermal stability. In contrast, Han and Langdon [25] gave proof that despite the fact that precipitates of θ' or θ are present in the AA 2219 aluminum alloy microstructure, they were not deemed powerful enough to inhibit the substantial growth of grain at high temperatures.

Nevertheless, to the best of our knowledge, no data dealing with the annealing behavior of the ECAPed AA6060 aluminum alloy have been reported until today. Accordingly, the current research aims to investigate the impact of annealing temperature on the microstructure morphology, texture and microhardness evolution of AA6060 aluminum alloy ECAPed up to eight ECAP passes.

2. Experimental procedure

The material studied is AA6060 aluminum alloy in the aged condition T6 as an extruded rod with a 10 mm diameter. Its detailed chemical composition has been reported elsewhere [14]. Rods were machined in about 60 mm long cylinders. The initial grain size was ~52 μm. ECAP was done using die with two channels that intersect at an angle of $\Phi = 90°$ and an outer curvature angle of $\Psi = 37°$. With this configuration, a total strain of 1 is impaired in each pass [26]. The ECAP processing

was done with a 0.02 m/s pressing velocity at room temperature. The lubricant used in the experiments was molybdenum disulfide (MoS2). Specimens were deformed up to eight ECAP passes through route B_C. Annealing treatments were conducted at various temperatures after ECAP: 150, 200, 250, 300, 350, 400 and 450 ° C for 1 hour under high vacuum, with a heating rate of 20 ° C min^{-1}.The microstructures of the specimens were examined through electron backscatter diffraction (EBSD) observations in the Scanning Electron Microscope (SEM) with a Field-Emission Gun (FEG) SUPRA 55 VP operating at 20 kV. For EBSD observations, all specimens were cut in the transverse direction (TD) plane from the core area and then mechanically polished from 1200 grit silicon carbide paper till 0.02µm colloidal silica, followed by electro-polishing utilizing Struers A2 electrolyte at 22 V. The examined regions were 100 x100 μm^2 with a step size of 0.1 µm for specimens annealed at 150 °C, and 200 x 200 μm^2 with a step size of 0.2 µm for specimens annealed at 250 °C, 300 °C, 350 °C and 450 °C. TSL Orientation Imaging Microscopy (OIM™) software was used to perform the EBSD data collection. Quantitative texture analysis was performed using the MTex software to calculate the pole figure (111) and the orientation distribution function (ODF). The ODF was measured using the harmonic approach (L equal to 22) with every orientation modeled with a Gaussian function possessing a 5 ° half-width. [27]. The linear intercept approach was used to calculate the mean grain size. The grain size values were determined with a 5 ° grain tolerance angle.

Vickers micro hardness of the specimens was characterized by SHIMADZU type HMV-2 tester using 100 g load (penetration time of 10 s) in the Extrusion Direction (ED)-Transversal Direction (TD) plane. At least 5 hardness indentations in the central regions of each specimen performed randomly.

3. Results and discussion

3.1. Microstructural evolution during annealing

Figures 1 to 4 demonstrate the TD inverse pole figure (TD-IPF) maps from EBSD illustrating the AA6060 alloy microstructures after 1, 2, 4 and 8 ECAP passes plus 1 h of annealing at the different temperatures considered. Low-angle grain boundaries (LAGB) and high-angle grain boundaries

(HAGB) were plotted with white and black lines whenever the misorientation angle was in range 2°-15° or exceeded 15°, respectively.

As reported earlier [15], with increasing ECAP passes, the microstructure evolved from a banded structure to a UFG one with elongated and smaller equiaxed grains mostly oriented along the shear direction. At lower recrystallization temperatures and strain (Figures 1c, 2c, and 3c), OIM maps display duplex microstructures characteristic of discontinuous recrystallization mechanism, clearly distinguishing deformed areas from recrystallized grains. At more advanced stages of recrystallization, i.e. larger ECAP passes (Figures 4d and 4e), the deformed structure's directionality is gradually lost. The microstructures arising from annealing 1 ECAP specimen show that the total recrystallization mechanism begins at a later stage compared to higher ECAP passes. Indeed, annealed at 150 and 250°C, the one and two pass samples (Figures 1a-1b and Figures 2a-2b) have retained almost the same microstructure as the deformed state. However, small recrystallized grains can be noticed in the large deformed grains and gathered in islands at grain boundaries (see the yellow square in Figure 2b) after annealing at 250°C. A similar observation can be found in the sample ECAPed four times at 250°C in a more advanced stage. According to Humphreys et al. [28], discontinuous recrystallization usually takes place on subsequent annealing for the greater original grain sizes and lower strains. Comparable retard in the recrystallization temperature has also been found by several authors [29,30].

As previously stated [15], annealing in the range of 100-500°C of AA6060 alloy processed by ECAP leads to the formation of solute rich clusters/Guinier-Preston (GP) zones and to an important reduction in the peak temperature correlated with the 50% of recrystallization with increasing ECAP passes. It was suggested that can impose a pinning impact (Smith-Zener pinning) on grain boundary in the annealed specimen after one ECAP pass, which prevents or retards the mechanism of recrystallization. Studying the recrystallization mechanism at particles in rolled aluminum, Humphreys [31] has deduced that the recrystallization arises with a random orientation at a pre-existing sub-grain

inside the deformation region. Then, the nucleation takes place by rapid sub-boundary migration. Finally, once the deformation zone is consumed, the grain growth may stop.

Complete recrystallization seems to occur after annealing at temperatures of 450, 300, 300, and 350°C for samples ECAPed once, twice, four and eight times, respectively as displayed at Figures 1e, 2c, 3c, and 4d. These results indicate that the kinetics of recrystallization significantly based on the strain imposed. It is well established that a rise in strain contributes to a rise in stored energy, which is the major driving energy for recrystallization. Consequently, the mechanism of recrystallization is accelerated. Inhomogeneous grain growth is obtained and some coarse grains can be observed in the EBSD maps at higher annealing temperatures (see Figures 1e, 2e, 3e, and 4e) due to the intense grain growth. However, some small regions with fine grains are still noted. As reported in the literature [32], the smaller grains are removed during annealing, while the larger grains grow, and the grain boundaries adopt a lower energy configuration. Under some conditions, through the mechanism of abnormal grain growth (secondary recrystallization), this normal grain growth can give way to the selective growth of a few large grains (Figure 3e, for example).

During annealing, changes in the relative proportions of HAGB were found to provide a valid way to determine the nature of the recrystallization mechanism [33]. As discontinuous recrystallization occurs, the HAGB fraction rises fairly rapidly, while the recrystallizing grains consume the deformed substructure. On the other hand, there is a slight shift in the HAGB fraction during continuous recrystallization [33]. The evolution of HAGB fraction during isochronal annealing is illustrated in Figure 5. HAGB fraction increases sharply and continually for the one pass specimen, at temperatures range between 250-300 °C in the 2 and 4 ECAP specimens and between 250 and 350 °C for the 8 ECAP passes specimen, indicating discontinuous recrystallization.

Nevertheless, despite a rise in the annealing temperature, it can be found that for the 4 ECAP specimen, the HAGB fraction remains nearly stable in the 300-450 °C temperature range and above 350 °C for the 2 and 8 ECAP passes specimens. This observation cannot indicate the occurrence of

continuous recrystallization since larger grains have been developed during recrystallization. Earlier observations [28,30], have suggested that continuous recrystallization occurs in specimens where a crucial HAGB fraction was formed during deformation (~64%). Thus, in the case of sufficiently large strains, the HAGB fraction rises to a reasonable value to maintain the microstructure against discontinuous recrystallization. In the present work, the AA6060 alloy has exhibited its maximum value of ~55% in HAGB fraction after deformation up to 8 ECAP passes [15] which seems to be insufficient to achieve continuous recrystallization.

Figures 6 and 7 summarize the grain size evolution and the recrystallized grains, respectively. Based on the grain orientation spread approach (GOS) available in OIM-software, the recrystallized grain fraction was determined. GOS represents the average deviation between every point orientation in the grain and the average grain orientation [34]. The recrystallized grains are distinct from the deformed ones by a threshold GOS value of 1° [35]. In the present study, GOS ≤1° are considered to be fully recrystallized.

As plotted in Figure 6, the average recrystallized grains is gradually increasing with rising annealing temperature. Initially, the measured grain sizes are marked by a stage of relatively slow evolution until 300 °C. Further annealing up to 450 °C shows a faster evolution, and the smallest grain size is obtained after 8 passes, which is inconsistent with several previous findings [29,36]. From this standpoint, it can be considered that the control of grain growth is more efficient after larger strain. According to Humphreys predictions [37], as the HAGB fraction produced on deformation increased, the microstructure gradually becomes stable against the catastrophic grains growth that bounded by HAGBs because of the energies and mobilities of HAGBs are not sensitive to boundary misorientation comparing to low angle boundaries. The average grain sizes after 1, 2, 4 and 8 ECAP passes after annealing at 450 ° C are approximately identical to 18 μm. This grain size is well below than the one of the as-received alloy (52 μm) [15] and could enhance its superplasticity ability.

The recrystallized grains fraction evolution in Figure 7 shows curves with a sigmoidal shape composing mainly of three distinct stages. The recrystallization fraction rate in the first stage ranges from 150 °C to 250 °C, and it grows slowly due to the incubation period. The second stage highlights a roughly considerable increase of the recrystallized grain fraction up to 350 °C. After that, a flat region with quite constant evolution takes place since the recrystallization is complete.

3.2 Texture evolution

3.2.1 Texture of the initial state

Figure 8 presents the texture of the as-received AA6060 alloy in terms of recalculated pole figure {111} and ODF section at φ_2 = 0 and 45°, respectively. The as-received alloy exhibits a typical extrusion texture, where a typical <001> fiber is formed. In this texture, the directions <001> are preferably aligned along the extrusion direction [38]. It also becomes apparent that the texture is dominated by the presence of components like Cube and Goss.

3.2.2 Texture evolution after ECAP and subsequent annealing

The ideal ECAP orientations for face-centered cubic (FCC) alloys utilizing a channel angle φ = 90° are presented and their characteristic positions in Euler space (φ_1,ϕ, φ_2) are given in Table 1. Figures 9-12 show the texture in term of recalculated pole figures (111) and ODF sections at φ_2 = 45° after ECAP via 1, 2, 4 and 8 ECAP passes and subsequent annealing for 1 h at 150, 250, 300, 350 and 450 °C, respectively. The ideal ECAP texture components are like the texture components for simple shear that are only rotated by 45° in comparison to the ECAP reference system [39].

Figure 9a indicates the development of a strong C component and weak B component after 1 ECAP pass. In addition, a very weak $\overline{B}$ component can be noticed in the ODF section (Figure 9a). The development of a strong C component during the first ECAP passes was already reported in ECAPed Copper and Al alloys using route B_C [40, 41].

These texture components seem to be stable until the 4 ECAP pass. Additionally, the ODF section of the sample extruded twice (Figure 11a) shows a weak $\overline{A}$ component. The intensity of the present orientations rises with rising the ECAP passes number up to 4 passes with a deviation from their ideal positions about 5–10° toward φ_1. This deviation is attributed to the effect of friction and dies geometry [39].

The presentation of ODF sections in the range of 0-360° in φ_1 revealed that the monoclinic symmetry is not evident. The monoclinic symmetry loss is frequently reported in route B_c due to a rotation around the ED axis between each pass [42]. After 8 ECAP passes, Figure 12 allows seeing significant texture changes. The texture intensity decreases and A component appears after annealing (Figure 12). This behavior leads to the formation of B fiber {hkl}<110> (containing the A, $\overline{A}$, B and $\overline{B}$ components) [39]. Conversely, the A fiber {111}<uvw> (containing A, $\overline{A}$, A_1^* and A_2^* components) [39] is not complete due to the absence of A_2^* component.

Molodova et al. [43] also reported the strengthening of C and B components with a rising ECAP passes number for UFG pure copper *via* route B_c. In the meantime, the domination of A_1^* was reported in copper, and Al-7075 alloy with increasing the number of ECAP passes using route B_c [42, 44]. Several authors [39, 44] reported that the texture components in route B_c are not stable (both in position and intensity) during the first 4 passes because of the complexity in the imposed deformation, which makes the texture characterization relatively tricky compared to route *A*. Accordingly, the development of the different shear texture components in the first ECAP passes strongly depends on the initial texture [39, 45, 46]. Thus, the ECAP processing with route B_c of material with strong <100> fiber leads to the development of a strong C component in the first passes [46]. This observation is in good agreement with the present finding, where the initial texture of the alloy developed a well-defined <100> fiber (Figure 9). The texture weakening with increasing ECAP passes was reported in

various FCC alloys processed by ECAP *via* route B_c [41, 42, 47]. According to some researchers [41], this texture evolution is attributed to the formation of new grains with different or random orientations.

The texture after 1 ECAP pass seems to be stable up to annealing at 350 °C for 1 h. As the annealing temperature rises, the C component remains the dominant texture although their intensities decrease. Interestingly, annealing at 450 °C leads to some changes in the texture of the specimen with one pass where C component tends to disappear and B to appear. The A-fiber and B-fiber are partially present due to the absence of $\overline{A}$ and $\overline{B}$ component. It is important to note that this typical ECAP texture was evaluated upon annealing at 300 °C in the 2 ECAP passes specimen and rapidly after annealing at 250 °C in case of the 4 ECAP passes specimen. The development of shear texture with decreasing annealing temperature could be attributed to the increase of stored energy introduced by high strain, thereby the acceleration of static recrystallization.

A significant shear texture weakening can be noticed in all annealed specimens. The texture weakening and randomization were also reported after annealing of deformed pure copper *via* route B_c with increasing ECAP passes [43]. Besides, intensity differences of $A/\overline{A}$ and $B/\overline{B}$ components are observed in the annealed samples implying the absence of the monoclinic symmetry.

The orientation changes during different annealing temperatures could be an indication of the discontinuous recrystallization occurrence. Indeed, it is well established that the evolution of the recrystallization texture is strongly related to the recrystallization mechanism [30,48]. The deformation texture was found retained during continuous recrystallization [36], while discontinuous recrystallization could lead to new orientations [49]. Indeed, the weakening of the recrystallization texture was associated with the appearance of large grains due to the occurrence of discontinuous recrystallization [43].

Figure 12 illustrates the texture during the isochronal annealing of the 8 ECAP pass specimen. This figure highlights that the texture intensity is higher than the other samples. The B, A and A_2^*

components disappeared upon annealing at 150 °C, and 250 °C. Figure 12d indicates a typical ECAP texture beginning from 300 °C.

The texture strengthening can be measured using the following equation [50]:

$$I = \frac{1}{8\pi^2}\int_G f^2(g).dg \quad (1)$$

where $f(g)$ is the ODF intensity at g orientation and G is the Euler space.

Figure 13 displays the texture index evolution against the annealing temperature of AA6060 alloy after ECAP processing and subsequent annealing.

This figure demonstrates that the texture indexes is almost stable during annealing up to 250 °C for all ECAPed samples, except for the 4 ECAP pass one where the texture index decreases rapidly from 8.5 to 3.2 upon annealing at 150 °C. The decrease in the texture strength can be noticed after annealing at 250 °C followed by stabilization until annealing at 450 °C where the texture index value is similar for almost all the ECAPed samples (~ 1.4).

3.3. Microhardness and dislocation density evolution after ECAP processing and annealing

Figure 14 shows the microhardness variation after annealing treatments. Before annealing, the microhardness values rise steadily with rising the ECAP passes number. The tendencies of microhardness-temperature relation for all specimens are similar, i.e., the microhardness values vary slightly till the temperature of 150 °C. Then, the microhardness sharply drops during annealing temperatures between 150 °C and 300 °C, and finally, it stabilizes for temperatures higher than 350 °C.

As shown in Figure 14, the microhardness of specimens after 1 and 2 passes undergo a gradual increase during annealing up to 150 °C. This evolution is related to the creation and the precipitation of solute rich clusters which create a pinning effect of precipitates on dislocations causing the strengthening of the material. An analysis of differential scanning calorimetry (DSC) carried out on the

identical material and under the identical ECAP conditions [15] demonstrated the presence of an exothermic peak in the range of 150-225 °C. This peak was associated with the GP zones precipitation.

A comparison with materials ECAPed 4 and 8 times revealed that the softening of these latter began at slightly lower annealing temperatures than the samples processed once and twice. In the range of temperature between 150-300 °C, the lowest microhardness value has been recorded for the four passes sample. In keeping with the rule of Johnson-Mehl-Avrami-Kolmogorov (JMAK) [51], this decrease becomes faster as the level of deformation rises. After registering almost the same microhardness values before annealing, the 8 ECAP pass sample seems to be more stable against annealing up to 300 °C having higher microhardness value than the 4 ECAP pass sample. The character of the curve indicates a shift in the process that governs the mechanical properties' deterioration. According to Hall–Petch relation [52,53], the strength of severely deformed UFGed material is affected mainly by the grain size and the dislocation densities [54]. Therefore, it is expected that the coarsening of grain and the elimination of dislocations during annealing would regulate the hardness and strength of the material. Figure 6, displaying the evolution of grain size, and Figure 15, displaying the evolution of dislocation density with isochronal annealing, need to be checked at the same time.

The Kernel Average misorientation (KAM) method characterizing the local misorientation is used to calculate the Geometrically Necessary Dislocations (GND) density in all the microstructure. Its principle is well explained in the literature [55]. From misorientation measurements, the density of dislocation (ρ_{GND}) can be calculated using the next equation [56-58]:

$$\rho_{GND} = \frac{\alpha\, \theta_{KAM}}{Xb} \tag{2}$$

where α is the parameter depending on the type of grain boundary and it is is equivalent to two for the tilting boundaries, four for twist ones and three for the mixture of the two types, X = nd is the kernel size (n the closest neighbors to be identified (n=3)) and d is the scan step (d=0.1 µm for specimens

annealed at 150 °C and d= 0.2 µm for specimens annealed at 250 to 450 °C) and b is the Burgers vector (b= 0.286 nm in aluminum).

The grain growth is negligible in the low temperature region (i.e.,150 °C-250 °C), while the dislocation density exhibits a dramatic collapse suggesting regeneration of the dislocation structure associated with UFG structure creation. In this temperature region, the most likely re-arrangement and mutual annihilation of dislocations with opposite signs occur during annealing. This observation ties well with earlier reports [59,60]. The fine grain structure is unstable during annealing and the grain sizes of recrystallized grains increase at temperatures 250 < T < 300 °C (see Figure 6). For all samples, the dislocation density declines abruptly in the same temperature range. Indeed, both dislocations annihilation and coarsening of grain are considered to contribute concurrently to the alloy softening. At elevated temperatures (T > 350 °C), the grain growth is likely to greatly affect the hardness of the studied alloy because no significant change occurs on dislocation density evolution.

3.4 Grain Growth Kinetics

The mechanism of grain growth requires a specific driving force, which is either supplied by diverse microstructural modifications (recrystallization, precipitate evolution, annihilation) or by external heat sources. Thus, normal grain growth is commonly characterized by a form relationship. [61]:

$$d^2 - d_0^2 = k\,t \tag{3}$$

where d is the mean grain size after annealing, d_0 is the original grain size [15], t is the annealing duration (where t=1h is used in those studies) and k is a parameter that describes the mobility of the grain boundary and the interface. The grain growth rate is correlated with the factor of boundary mobility (k) and can be calculated through the use of the conventional Arrhenius equation [61]:

$$k = A\exp\left(\frac{-Q}{RT}\right) \tag{4}$$

where *A* is a pre-exponential constant, *R* is the gas constant, *Q* is the activation energy for boundary mobility that is correlated with the driving force needed to activate grain growth, and *T* is the absolute temperature of annealing.

The present data can be interpreted by constructing the plot of ln ($\frac{d^2 - d_0^2}{t}$) versus l000/RT. Figure 16 represents the annealing influence on grain growth kinetics of AA6060 alloy. This plot allows distinguishing two temperature ranges with different activation energies. The difference in the rate of grain growth from lower to higher temperatures, which reveals distinct growth regimes, has been extensively reported in the literature [61-65]. At low annealing temperature (T < 300 °C), Q is the energy needed for complete recrystallization of the unrecrystallized microstructure, while at the elevated annealing temperature (T > 300 °C) Q is the activation energy for coarsening of the initial UFG microstructure [65].

One can easily observe that the activation energy continually reduces with increasing ECAP passes. A similar observation was obtained earlier [43,66]. This finding was correlated with a rise in HAGBs fraction with an increasing ECAP passes number allowing less activation energy of recrystallization.

The main activation energy (*Q*) determined from the slopes of the experimental results in the unrecrystallized grains at lower temperatures (≤ 300 °C), is about ~ 75 kJ mol^{-1}. This value is significantly smaller than the predicted value for lattice self diffusion in pure Al (~143.4 kJ mol^{-1}[67]), or the activation energy for Mg impurity diffusion in Al (~130.5 kJ mol^{-1}[68]), neither that for lattice diffusion of Si in Al (~125-154 kJ mol^{-1} [69]). However, it is quite closer to the value expected for grain boundary diffusion in Al (~86 kJ mol^{-1}[67]) and that for diffusion across dislocation cores in Al (~82 kJ mol^{-1}[70]). Previous studies have claimed that low activation energy for grain boundary diffusion could be accomplished in SPD-produced UFG materials. One reason is that the non-equilibrium grain boundaries are unstable requiring a slight additional driving force to allow the grains and grain boundaries to be rearranged [71,72]. Other researchers attributed the low energies to the

improved atomic mobility of the nonequilibrium grain boundaries owing to the enhanced diffusivity resulting from the existence of multiple extrinsic dislocations [73]. Besides, aluminum with its strong stacking fault energy favors the dislocation annihilation and offers the required driving force for the annihilation of dislocation and recrystallization [74].

The activation energy is unexpectedly low (~20 $kJmol^{-1}$) in the completely recrystallized structure at high temperatures (> 300 °C). This value is inconsistent with numerous findings in the literature obtained after several SPD techniques of different Al alloys like Al-Mg processed by ECAP [61], AA6061 subjected to ARB [63], AA5083 fabricated by cryo-milling [65] or AA2014 processed by cryo-rolling [65]. Nevertheless, several other studies suggest a similar change to a high-temperature regime with very low activation energy [75-78]. E.g., studying the thermal stability of AA6061 aluminum alloy developed by cryo-rolling followed by optimal aging heat treatment [75], it has been recorded a decrease in the activation energy in the elevated temperature range (300-500 °C). They attributed to the dissolution of coherent and semi-coherent precipitates and to the diminution in the pinning impact that inhibits the migration of grain boundaries and then the amount of activation energy. Likewise, there have been reports of a change to quite a low activation energy in an elevated temperature regime which is near to that for boundary diffusion in high purity lead [76] and to that for liquid diffusion in zinc [77]. The first study [76] has suggested the occurrence of change to various boundary structure. Nevertheless, in the second investigation [77], the low energy was described as a transition in the boundary migration process from one dominated by diffusion to other requiring collaborative shuffles of atomic. Recently, a one grain growth regime was observed in the AA7075 alloy treated by ultrasonic shot peening and annealed at different temperatures up to 350°C where the activation energy for grain growth was determined to be 37.9 $kJmol^{-1}$ [78]. The latter research considered that the dominant role in grain coarsening was played by grain boundary self-diffusion.

Grain growth requires the migration of HAGBs and the kinetics are strongly influenced by many factors, including solute (impurity) drag, second phase (Zener) drag, the temperature dependence

of grain boundary mobility, and grain boundary segregation [78, 79]. The driving force for grain growth is typically quite low at high temperatures, particularly in comparison to the recrystallization regime [80].

Conclusion

Series of AA6060 alloy samples for thermal stability investigations were subjected through Equal Channel Angular Pressing using the Route *Bc* for 1, 2, 4 and 8 passes and followed by isochronal annealing at various temperatures range between 150 and 450 °C for 1 h.

The following conclusions were drawn.

- The specimens showed recrystallization and grain growth. In addition, the recrystallized microstructure typically has the randomly scattered large grains and small grains indicating the appearance of the discontinuous recrystallization process.
- ECAP process through 1, 2, and 4 ECAP passes lead to the development of strong C component and weak B component. Meanwhile, the typical shear ECAP texture of FCC metals is observed after 8 ECAP passes. The texture intensity increases with increasing ECAP processing up to 4 passes and then decreases after 8 ECAP passes. The calculation of the texture index shows the propensity for texture weakening and randomization with rising annealing temperature up to 450 °C.
- It was noticed from the observed transitions distinguished by sudden softening and degradation of the deformation texture components, which occurred after annealing above 150°C while the UFG microstructure of the AA6060 ECAPed material remained stable up to this temperature.
- The 8 ECAP pass sample has shown a limited grain growth and a restricted evolution after 300°C. A relatively homogeneous microstructure after annealing up to 450 °C has been obtained with reasonably small mean grain size ~ 12.5 µm compared to the 4 ECAP pass sample (~16 µm) despite their similar behavior after ECAP processing in terms of achieved grain sizes (0.57 and 0.68 µm, respectively).

- The grain growth kinetics of AA6060 alloy are followed by two stages that rely upon the range of annealing temperature. Average order values of ~75 and ~20 kJ mol^{-1} of activation energies were estimated in the elevated temperature 300–450 °C range and the low temperature 150-300 °C range, respectively. At elevated temperatures, the grain growth is controlled by lattice self diffusion. While at low temperatures, the grain growth is governed by high mobility of the nonequilibrium grain-boundary.

Acknowledgments

Tarek khelfa and Fuguo Li acknowledge the financial support of the National Natural Science Foundation of China (Grant No. 51275414, No.51605387). This work also was supported by the PHC-Maghreb program N° 16MAG03.

JMC thanks CONACYT (Mexico) for the economic partial funding of his sabbatical leave at UMSNH.

JAMB gratefully acknowledges the financial support of the Ministry of Science and Higher Education of the Russian Federation in the framework of Increase Competitiveness Program of NUST «MISiS» (No. К4-2019-045), implemented by a governmental decree dated 16th of March 2013, N 211.

Data availability

The raw/processed data required to reproduce these findings cannot be shared at this time as the data also forms part of an ongoing study.

References

[1] R.Z. Valiev, K. Islamgaliev, I.V. Alexandrov, Bulk nanostructured materials from severe plastic deformation. Prog Mater Sci, 45 (2000) 103-189.

[2] R.Z. Valiev, N.A. Krasilnikov, N.K. Tsenev, Plastic deformation of alloys with submicron-grained structure. Mater Sci Eng A, 137 (1991) 35-40

[3] R.Z. Valiev, A.V. Korznikov, R.R. Mulyukov, Structure and properties of ultrafine-grained materials produced by severe plastic deformation. Mater Sci Eng A, 168 (1993) 141-148.

[4] R.Z.Valiev, T.G. Langdon, Principles of equal-channel angular pressing as a processing tool for grain refinement. Prog Mater Sci, 51 (2006) 881-981.

[5] V.M. Segal, V.I. Reznikov, A.E. Drobyshevski, V.I. Kopylov, Plastic working of metals by simple shear. Russ Metall 1 (1981) 99-105.

[6] T. Inoue, R. Ueji, Improvement of strength, toughness and ductility in ultrafine-grained low-carbon steel processed by warm bi-axial rolling. Mater Sci Eng A,786 (2020) 139415.

[7] M. Naseri , M. Reihanian, E. Borhani, Effect of strain path on microstructure, deformation texture and mechanical properties of nano/ultrafine grained AA1050 processed by accumulative roll bonding (ARB). Mater Sci Eng A, 673 (2016) 288-298.

[8] E.V. Bobruk, V.U. Kazykhanov, M.Y. Murashkin, R.Z. Valiev, Enhanced strengthening in ultrafine-grained Al-Mg-Si alloys produced via ECAP with parallel channels. Adv. Eng. Mater. 17 (2015) 1733-1737.

[9] W. Yuan, Z. Liang, C. Zhang, L. Wei, Effects of La addition on the mechanical properties and thermal-resistant properties of Al-Mg-Si-Zr alloys based on AA 6201. Mater. Des, 34 (2012) 788-792.

[10] X. Ji, H. Zhang, S. Luo, F. Jiang, D. Fu, Microstructures and properties of Al-Mg-SI alloy overhead conductor by horizontal continuous casting and continuous extrusion forming process, Mater. Sci. Eng. A 649 (2016) 128-134.

[11] M.Y. Murashkin, I. Sabirov, V.U. Kazykhanov, E.V. Bobruk, A.A. Dubravina, R.Z. Valiev, enhanced mechanical properties and electrical conductivity in ultrafine-grained Al alloy processed via ECAP-PC, J. Mater. Sci. 48 (2013) 4501-4509.

[12] W.J. Kim, C.S. Chung, D.S. Ma, S.I. Hong, H.K. Kim, Optimization of strength and ductility of 2024 Al by equal channel angular pressing (ECAP) and post-ECAP aging. Scr Mater 49 (2003) 333-338.

[13] Z. Horita, T. Fujinami, M. Nemoto, T.G. Langdon, Equal channel angular pressing of commercial aluminum alloys: grain refinement, thermal stability and tensile properties. Metall Mater Trans A, 31 (2000) 691-701.

[14] T. Khelfa, M. A. Rekik, M. Khitouni, J. M. Cabrera-Marrero, Structure and microstructure evolution of Al–Mg–Si alloy processed by equal-channel angular pressing. Int J Adv. Manuf. Techn. 92 (2017) 1731-1740.

[15] T. Khelfa, M. A. Rekik, J. A. Muñoz-Bolaños, J. M. Cabrera-Marrero, M. Khitouni. Microstructure and strengthening mechanisms in an Al-Mg-Si alloy processed by equal channel angular pressing (ECAP). Int J Adv. Manuf. Techn, 95 (2018) 1165-1177.

[16] Ningning Liang, Yonghao Zhao, Y. Li, T. Topping, Yuntian Zhu, R. Z. Valiev & E. J. Lavernia, Influence of microstructure on thermal stability of ultrafine-grained Cu processed by equal channel angular pressing. J Mater Sci, 53 (2018) 13173-13185.

[17] N. Rangaraju, T. Raghuram, B.V. Krishna, K.P. Rao, P. Venugopal, Effect of cryo-rolling and annealing on microstructure and properties of commercially pure aluminium, Mater. Sci. Eng. A, 398 (2005) 246-251.

[18] J.A. Muñoz, O.F. Higuera, A. Hernández-Expósito, A. Boulaajaj, R. E. Bolmaro, F.D. Dumitru, P. Rodriguez-Calvillo, A. Moreira Jorge, J.M. Cabrera. Thermal stability of ARMCO iron processed by ECAP. Int J Adv. Manuf. Techn, 98 (2018) 2917-2932.

[19] A. Hanna, H. Azzeddine, Y. Huang, D. Bradai, J.M. Cabrera, T.G. Langdon, An investigation of the thermal stability of a Mg-Dy alloy after processing by high-pressure torsion. Mater. Charact, 151 (2019) 519-529.

[20] N. Lugo, N. Llorca, J.J. Suñol, J.M. Cabrera, Thermal stability of ultrafine grains size of pure copper obtained by equal-channel angular pressing, J. Mater. Sci, 9 (2010) 2264-2273.

[21] J. Mao, S.B. Kang, J.O. Park, Grain refinement, thermal stability and tensile properties of 2024 aluminum alloy after equal-channel angular pressing, J. Mat. Proc. Tech. 159 (2005) 314-320.

[22] I. Nikulin, R. Kaibyshev, The Effect of Temperature on Microstructure Evolution in a 7055 Aluminum Alloy Subjected to ECAP. Mater. Sci. Forum, 715-716 (2012) 317-322.

[23] A. Dhal, S.K. Panigrahi, M.S. Shunmugam, Precipitation phenomena, thermal stability and grain growth kinetics in an ultra-fine grained Al 2014 alloy after annealing treatment. J.Alloy.Compd, 649 (2015) 229-238.

[24] P.B. Prangnell, J.S. Hayes, J.R. Bowen, P.J. Apps, P.S. Bate, Continuous recrystallisation of lamellar deformation structures produced by severe deformation. Acta.Mater, 52 (2004) 3193-3206.

[25] B.Q. Han, T.G. Langdon, Significance of microstructural thermal stability in an Al-2219 alloy processed by severe plastic deformation, Ultrafine Grained Materials II (Y.T. Zhu, T.G. Langdon, R.S. Mishra, S.L. Semiatin, M.J. Saran, T.C. Lowe, eds.), 485-494. The Minerals, Metals and Materials Society, Warrendale, PA (2002).

[26] Y. Iwahashi, J. Wang, M. Horita, M. Nemoto, T.G. Langdon, Principle of equal-channel angular pressing for the processing of ultra-fine-grained materials. Scr. Mater, 35 (1996) 143-146.

[27] F. Bachmann, R. Hielscher, H. Schaeben Texture analysis with MTEX. Solid State Phenom, 160 (2010) 6-68.

[28] F.J. Humphreys, G.S. Rohrer, A Rollett, chapter 14 - continuous recrystallization during and after large strain deformation, in F.J. Humphreys, G.S. Rohrer, A Rollett (Eds,), Recrystallization and related annealing phenomena (third edition),, Elsevier, Oxford, 2017, pp. 509-526.

[29] S. Ferrasse, V.M. Segal, F. Alford, Texture evolution during equal channel angular extrusion (ECAE): part II. An effect of post-deformation annealing. Mater. Sci. Eng. A372 (2004) 235-244.

[30] H. Jazaeri, F.J. Humphreys, The transition from discontinuous to continuous recrystallization in some aluminium alloys: I - the deformed state. Acta Mater. 52 (2004) 3239–3250.

[31] F.J. Humphreys, The nucleation of recrystallization at second phase particles in deformed aluminium. Acta Metall. 25, (1977) 1323-1344.

[32] F.J. Humphreys, M. Hatherly, chapter 1- Introduction, in: F.J. Humphreys, M. Hatherly (Eds.), Recrystallization and related annealing phenomena. (second edition),, Oxford, Elsevier, 2004. pp,1-10.

[33] H. Jazaeri,F.J. Humphreys, Quantifying recrystallization by electron backscatter diffraction. J Microsc, 213 (2004) 241-246.

[34] O.Wouters, W. Vellinga, V.R. Tijum, D.J.T.M. Hosson, Effects of crystal structure and grain orientation on the roughness of deformed polycrystalline metals. Acta Mater, 54 (2006) 2813-2821.

[35] J.H. Cho, A. Rollett, K. Oh, Determination of a mean orientation in electron backscatter diffraction measurements. Metall. Mater. Trans. A, 36 (2005) 3427-3428.

[36] K. Abib, H. Azzeddine, K. Tirsatine, T. Baudin, A-L. Helbert, F. Brisset, B. Alili, D. Bradai. Thermal stability of Cu-Cr-Zr alloy processed by equal-channel angular pressing Mater.Charact, 118 (2016) 527-534.

[37] F.J. Humphreys, A unified theory of recovery, recrystallization and grain growth, based on the stability and growth of cellular microstructures-I. The basic model, Acta Mater, 45 (1997) 4231-4240.

[38] J. Hirsch, Texture and Anisotropy in Industrial Applications of Aluminum Alloys. Arch Metall Mater, 50 (2005) 21-34.

[39] I.J. Beyerlein, L.S. Toth, Texture evolution in equal-channel angular extrusion, Prog Mater Sci 54 (2009) 427-510.

[40] O.F. Higuera, J.M. Cabrera, Texture Analysis in Ultrafine Grained Coppers Processed by Equal Channel Angular Pressing. Mater. Res,16 (2013) 619-624.

[41] C. Reyes-Ruiz, I. A. Figueroa, C. Braham, J.M. Cabrera, I. Alfonso, G. Gonzalez. Texture and Lattice Distortion Study of an Al-6061-T6 Alloy Produced by ECAP. Mater. Trans, 56 (2015) 1781-1786.

[42] M.H. Shaeri, M. Shaeri, M.T. Salehi, S.H. Seyyedein, F. Djavanroodi. Microstructure and texture evolution of Al-7075 alloy processed by equal channel angular pressing. Trans. Nonferrous Met. Soc. China, 25(2015) 1367-1375.

[43] X. Molodova, G. Gottstein, M. Winning, R.J. Hellmig. Thermal stability of ECAP processed pure copper. Mater. Sci. Eng. A, 460-461 (2007) 204-213.

[44] S. Li, I. J. Beyerlein, D. J. Alexander, S. C. Vogel. Texture evolution during multi-pass equal channel angular extrusion of copper: Neutron diffraction characterization and polycrystal modeling. Acta. Mater, 53 (2005) 2111-2125.

[45] S. Li. I.J. Beyerlein, D.J. Alexander, S. C. Vogel, Texture evolution during equal channel angular extrusion: Effect of initial texture from experiment and simulation. Scripta Mater, 52 (2005) 1099-1104.

[46] S. Suwas, R. Arruffat-Massion, L.S. Tóth, A. Eberhardt, J.J.Fundenberger, W.Skrotzki, Evolution of crystallographic texture during equal channel angular extrusion of copper: The role of material variables. Metall. Mat.Trans. A 37 (2006) 739-753.

[47] K. Abib, J. A. Munoz Balanos, B. Alili, D. Bradai, On the microstructure and texture of Cu-Cr-Zr alloy after severeplastic deformation by ECAP. Mater Charact, 112 (2016) 252-258.

[48] H. Jazaeri, F.J. Humphreys, The transition from discontinuous to continuous recrystallization in some aluminium alloys: II – annealing behavior, Acta.Mater, 52 (2004) 3251-3262.

[49] K. Tirsatine, H. Azzeddine, T. Baudin, A-L.Helbert, F. Brisset, D. Bradai, On the recrystallization and texture of Fe-36%Ni alloy after accumulative roll bonding and annealing at 600 °C. Mater. Eng, 24 (2017) 56-66.

[50] H.J. Bunge. Texture Analysis in Materials Science: Mathematical Methods, Butterworth & Co, London, 1982.

[51] F.J. Humphreys, M. Hatherly, Recrystallisation and Related Annealing Phenomena, Pergamon, Oxford, UK, 1995, p.451.

[52] E.O. Hall, The deformation and ageing of mild steel: III discussion of results. Proc R Soc, B64 (1951) 747-753.

[53] N.J. Petch, The cleavage strength of polycrystals. J Iron Steel Inst, 174 (1953) 25-28.

[54] Y. Estrin. L.S. Tóth,A. Molinari,Y. Bréchet, A dislocation-based model for all hardening stages in large strain deformation. Acta Mater, 46 (1998);:5509-5522.

[55] Y.A.Betanda, A.L. Helbert, F. Brisset, M.H. Mathon,T. Waeckerlé, T.Baudin, Measurement of stored energy in Fe-48%Ni alloys strongly cold-rolled using three approaches: Neutron diffraction, Dillamore and KAM approaches.Mater. Sci. Eng A, 614(2014)193-198.

[56] Y. Takayama, J. Szpunar, Stored energy and Taylor factor relation in an Al-Mg-Mn alloy sheet worked by continuous cyclic bending. Mater. Trans, 45 (2004) 2316-2325.

[57] Q. Liu, D. Juul Jensen, N. Hansen, Effect of grain orientation on deformation structure in cold-rolled polycrystalline aluminium. Acta.Mater, 46 (1998) 5819-5838.

[58] M. Calcagnotto, D. Ponge, E. Demir, D. Raabe, Orientation gradients and geometrically necessary dislocations in ultrafine grained dual-phase steels studied by 2D and 3D EBSD, Mater. Sci. Eng. A, 527 (2010) 2738-2746.

[59] J Stráská, M Janeček, J Čížek, J Stráský, B Hadzima, Microstructure stability of ultra-fine grained magnesium alloy AZ31 processed by extrusion and equal-channel angular pressing (EX–ECAP). Mater. Charact, 94 (2014) 69 -79.

[60] A. Zi, I. Stulikova, B. Smola, Response of aluminum processed by extrusion preceded ECAP to isochronal annealing. Mater Sci Eng A, 527 (2010) 1469-1472.

[61] J. Wang, Y. Iwahashi, Z. Horita, M. Furukawa, M. Nemoto, R. Z. Valiev, T. G. Langdon, An Investigation of Microstructural Stability in An Al-Mg Alloy with Submicrometer Grain Size. Acta mater, 44 (1996) 2973-2982.

[62] S. Tighiouaret, R. Lachhab, A. Hanna, H. Azzeddine, Y. Huang, T. Baudin, A-L. Helbert, F. Brisset, D. Bradai, T.G. Langdon, Thermal Stability of an Mg–Nd Alloy Processed by High-Pressure Torsion. Adv. Eng. Mater, 21 (2019) 1900801

[63] K.T. Park, H.J. Kwon, W.J. Kim, Y.S. Kim, Microstructural characteristics and thermal stability of ultrafine grained 6061 Al alloy fabricated by accumulative roll bonding process. Mater. Sci. Eng. A 316 (2001) 145-152.

[64] F.A. Mohamed, T.G. Langdon, Deformation mechanism maps based on grain size. Metall. Trans. 5 (1974) 2339-2345.

[65] A. Dhal, S.K. Panigrahi, M.S. Shunmugam, Insight into the microstructural evolution during cryo-severe plastic deformation and post-deformation annealing of aluminum and its alloys. J. Alloys Compd, 726 (2017) 1205-1219.

[66] O.F. Higuera-Cobos, J.M. Cabrera, Mechanical, microstructural and electrical evolution of commercially pure copper processed by equal channel angular extrusion. Mater. Sci. Eng. A 571 (2013) 103-114

[67] F. A. Mohamed and T. G. Langdon, Deformation mechanism maps based on grain size. Metall. Trans, 5 (1974) 2339-2345.

[68] S. J., Rothman, N. L. Peterson, L. J. Nowicki and L. C. Robinson, Tracer Diffusion of Magnesium in Aluminum Single Crystals. Phys. Status Solidi B, 63, (1974) K29-K33.

[69] Y. Huang, F.J. Humphreys, Subgrain growth and low angle boundary mobility in aluminium crystals of orientation {110}〈001. Acta Mater, 48 (2000) 2017-2030.

[70] L.E. Murr, 1975. Interfacial Phenomena in Metals and Alloys. Addison-Wesley, Reading, p. 131.

[71] R. Z. Valiev, E. V. Kozlov, Yu. F. Ivanov, J. Lian, A. A. Nazarov, B. Baudelet, Deformation behaviour of ultra-fine-grained copper, Acta Metall. Mater. 42 (1994) 2467-2475.

[72] J. Lian, R. Z. Valiev and B. Baudelet, On the enhanced grain growth in ultrafine grained metals. Acta Metall. Mater. 43 (1995) 4165-4170.

[73] I. Roy, M. Chauhan, E. J. Lavernia, F A. Mohamed, Thermal Stability in Bulk Cryomilled Ultrafine-Grained 5083 Al Alloy. Metall Mater Trans A, 37 (2006) 721–730.

[74] A. Dhal, S.K. Panigrahi, M.S. Shunmugam Precipitation phenomena, thermal stability and grain growth kinetics in an ultra-fine grained Al 2014 alloy after annealing treatment. J. Alloys Compd, 649 (2015) 229-238.

[75] M. Abbasi-Baharanchi, F. Karimzadeh, M. H. Enayati Thermal Stability Evaluation of Nanostructured Al6061 Alloy Produced by Cryorolling Trans. Nonferrous Met. Soc. China, 27 (2017) 754-762.

[76] H. Gleiter, Observations suggesting a transformation in the structure of high-angle grain boundaries in lead. Z. Metallkd, 61 (1970) 282-287.

[77] P. Gondi, R. Montanari,, A. Sili, A. 1992. In: Abbruzzeze, Brozzo (Eds.), Grain Growth in Polycrystalline Materials. Trans. Tech. Publ., Switzerland, p. 591.

[78] V. Pandey, K. Chattopadhyay, N.C. SanthiSrinivas, V. Singh, Thermal and microstructural stability of nanostructured surface of the aluminium alloy 7075 Mater. Charact, 151 (2019) 242-251.

[79] Y. Liu, B. Jin, J. Lu, Mechanical properties and thermal stability of nanocrystallized pure aluminum produced by surface mechanical attrition treatment. Mater. Sci. Eng. A, 636 (2015) 446–451.

[80] J. Humphreys, G.S. Rohrer, A. Rollett, chapter 11 - Grain Growth Following Recrystallization in; J.Humphreys, G.S. Rohrer, A. Rollett (Eds,), Recrystallization and related annealing phenomena (third edition), Elsevier, Oxford, 2017, pp. 375-429.

Figures captions

Figure 1: IPF maps of AA6060 after 1 ECAP passes and subsequent annealing for 1 h at: (a) 150 °C, (b) 250 °C, (c) 300 °C, (d) 350 °C and (e) 450 °C.

Figure 2: IPF maps of AA6060 after 2 ECAP passes and subsequent annealing for 1 h at: (a) 150 °C, (b) 250 °C, (c) 300 °C, (d) 350 °C and (e) 450 °C.

Figure 3: IPF maps of AA6060 after 4 ECAP passes and subsequent annealing for 1 h at: (a) 150 °C, (b) 250 °C, (c) 300 °C, (d) 350 °C and (e) 450 °C.

Figure 4: IPF maps of AA6060 after 8 ECAP passes and subsequent annealing for 1 h at: (a) 150 °C, (b) 250 °C, (c) 300 °C, (d) 350 °C and (e) 450 °C.

Figure 5: Volume fraction of HAGBs of AA6060 processed by ECAP through 1, 2, 4 and 8 passes as function of annealing temperature.

Figure 6: Recrystallized grain size evolution of AA6060 processed by ECAP through 1, 2, 4 and 8 passes as function of annealing temperature.

Figure 7: Evolution of the recrystallized grain percentage of AA6060 processed by ECAP through 1, 2, 4 and 8 passes as function of annealing temperature.

Figure 8: Recalculated pole figure (111) and ODF sections at φ_2 = 0 and 45° of the as-received AA6060 alloy.

Figure 9 : Recalculated pole figure (111) and ODF section at φ_2 = 45° of AA6060 alloy after: a) 1 ECAP pass and subsequently annealing for 1 h at : b) 150 °C, c) 250 °C, d) 300 °C, e) 350 °C and f) 450 °C.

Figure 10 : Recalculated pole figure (111) and ODF section at φ_2 = 45° of AA6060 alloy after: a) 2 ECAP passes and subsequently annealing for 1 h at : b) 150 °C, c) 250 °C, d) 300 °C, e) 350 °C and f) 450 °C.

Figure 11: Recalculated pole figure (111) and ODF section at φ_2 = 45° of AA6060 alloy after: a) 4 ECAP passes and subsequently annealing for 1 h at : b) 150 °C, c) 250 °C, d) 300 °C, e) 350 °C and f) 450 °C.

Figure 12: Recalculated pole figure (111) and ODF section at φ_2 = 45° of AA6060 alloy after: a) 8 ECAP passes and subsequently annealing for 1 h at : b) 150 °C, c) 250 °C, d) 300 °C, e) 350 °C and f) 450 °C.

Figure 13: Evolution of the texture index before and after annealing.

Figure 14: Hardness evolution the of AA6060 alloy processed by ECAP through 1, 2, 4 and 8 passes as a function of annealing temperature.

Figure 15: Evolution of the dislocation density in AA6060 alloy as a function of annealing temperature.

Figure 16: : Evolution of $\ln(d^2-d_0^2/t)$ as a function of 1000/RT for AA6060 alloy processed by ECAP and subsequent annealed:a) 1 pass, b) 4 passes, c) 4 passes, d) 8 passes.

Table captions

Table 1: Ideal ECAP orientations for FCC alloys using a channel angle φ of 90°

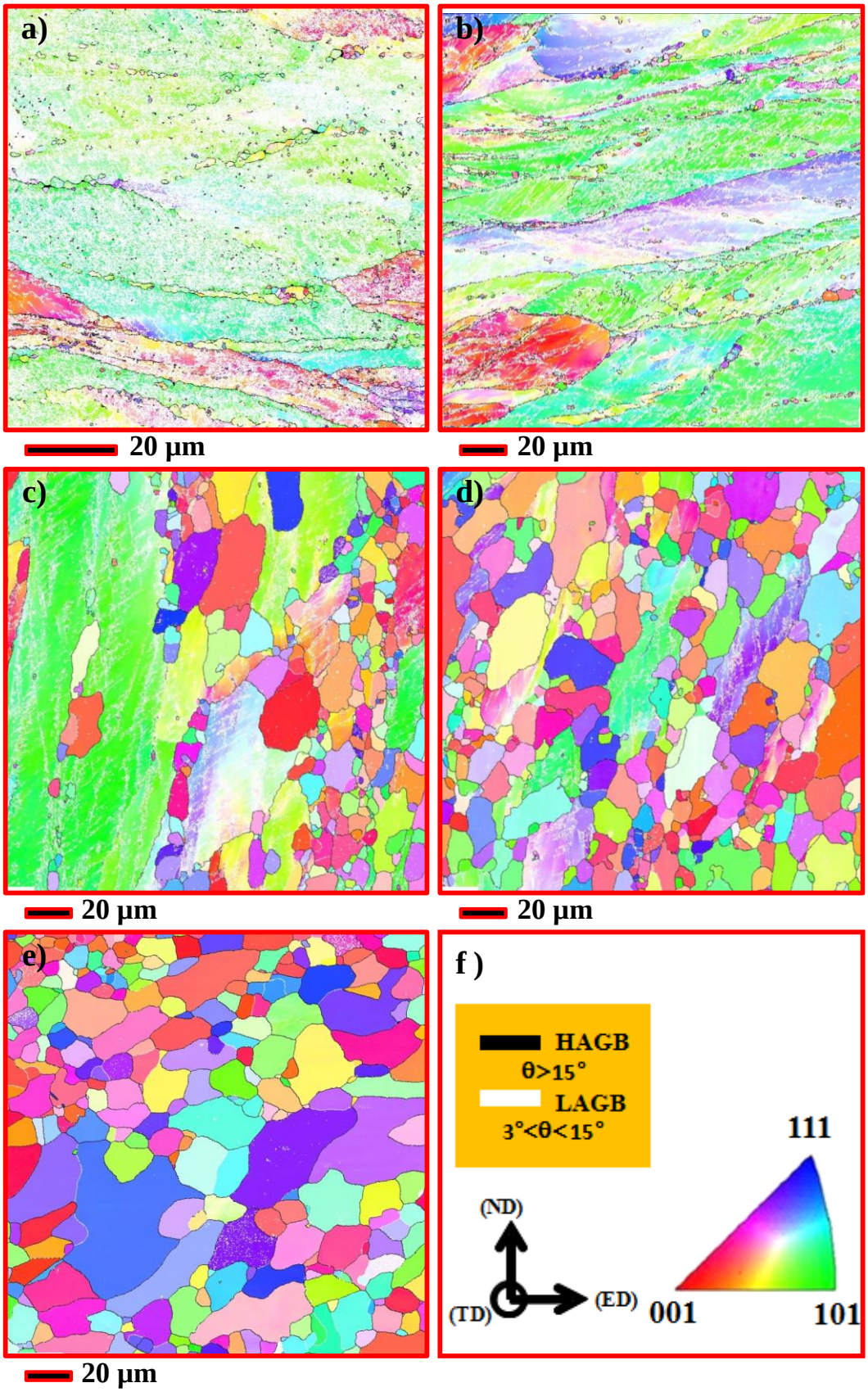
a)
20 µm
b)
20 µm
c)
20 µm
d)
20 µm
e)
20 µm
f)
HAGB
θ>15°
LAGB
3°<θ<15°
111
(ND)
(TD)
(ED)
001
101

Figure 1

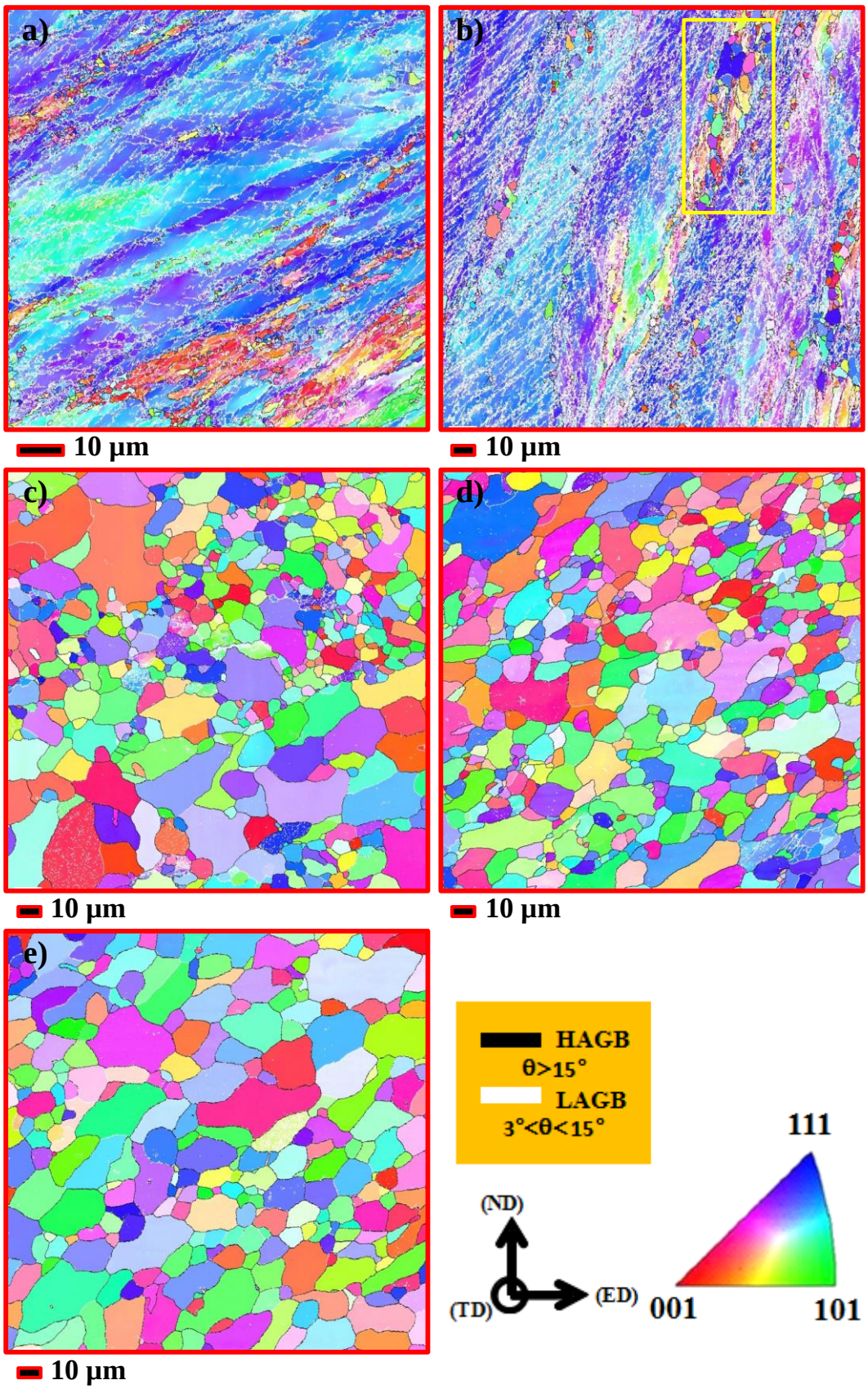
a)
b)
10 µm
10 µm
c)
d)
10 µm
10 µm
e)
10 µm
HAGB
θ>15°
LAGB
3°<θ<15°
(ND)
(TD)
(ED)
111
001
101

Figure 2

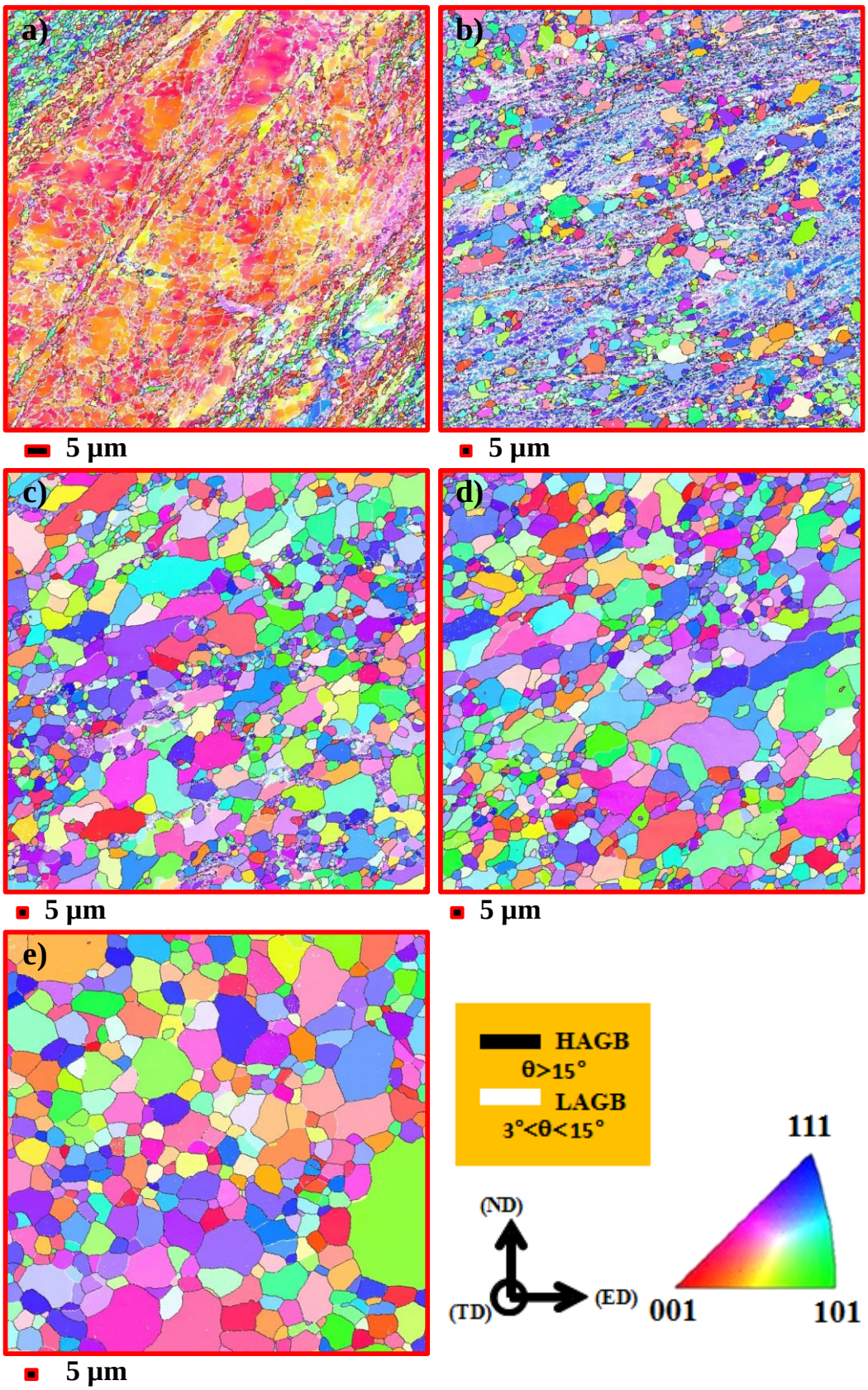
a)
b)
5 µm
5 µm
c)
d)
5 µm
5 µm
e)
5 µm
HAGB
θ>15°
LAGB
3°<θ<15°
(ND)
(TD)
(ED)
111
001
101

Figure 3

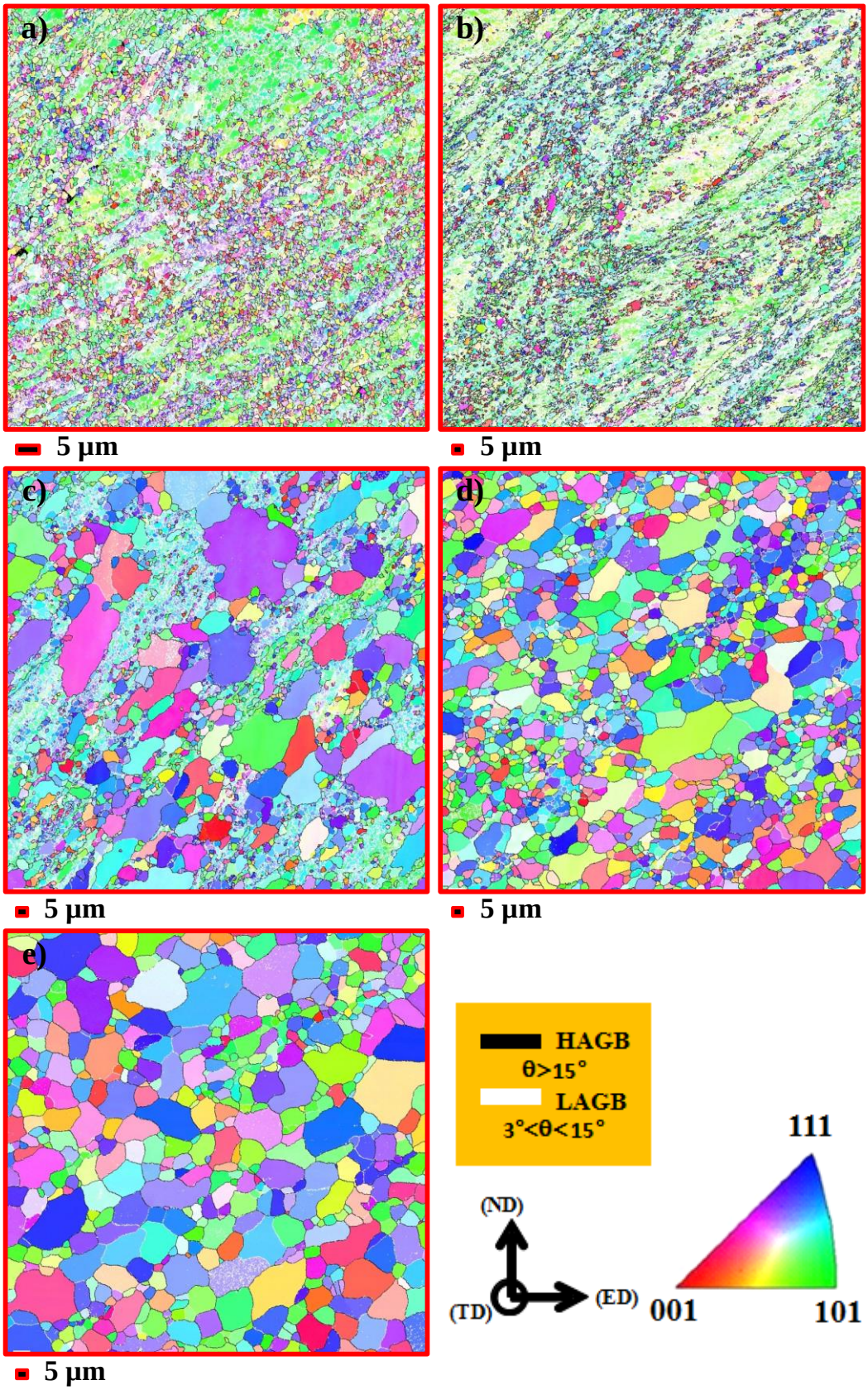
a)
b)
5 µm
5 µm
c)
d)
5 µm
5 µm
e)
5 µm
HAGB
θ>15°
LAGB
3°<θ<15°
(ND)
(TD)
(ED)
111
001
101

Figure 4

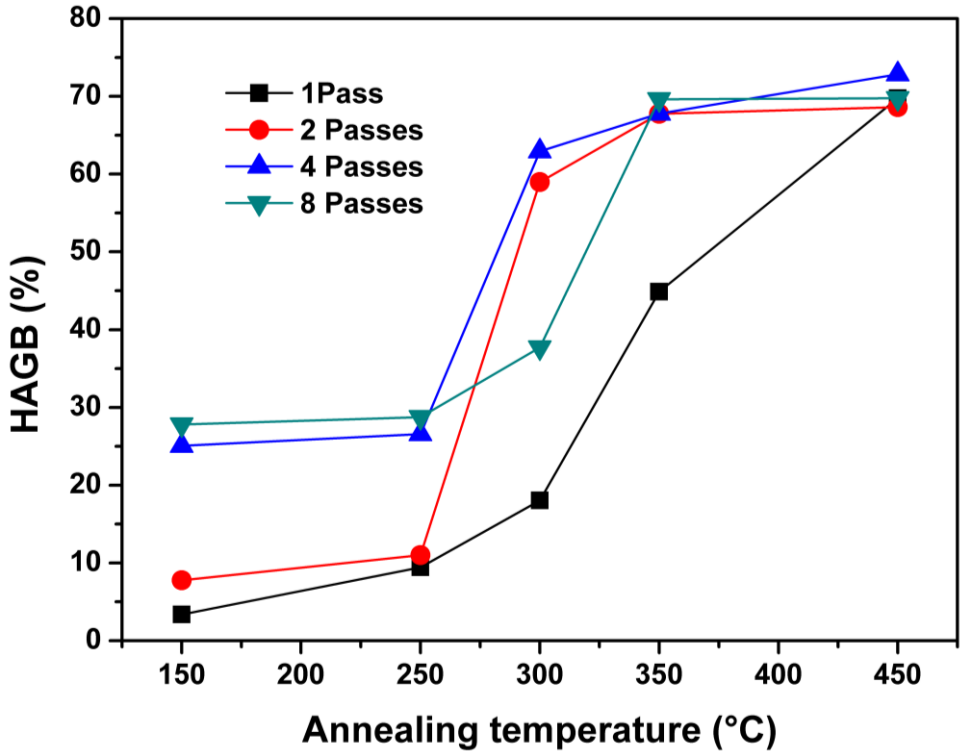

Figure 5

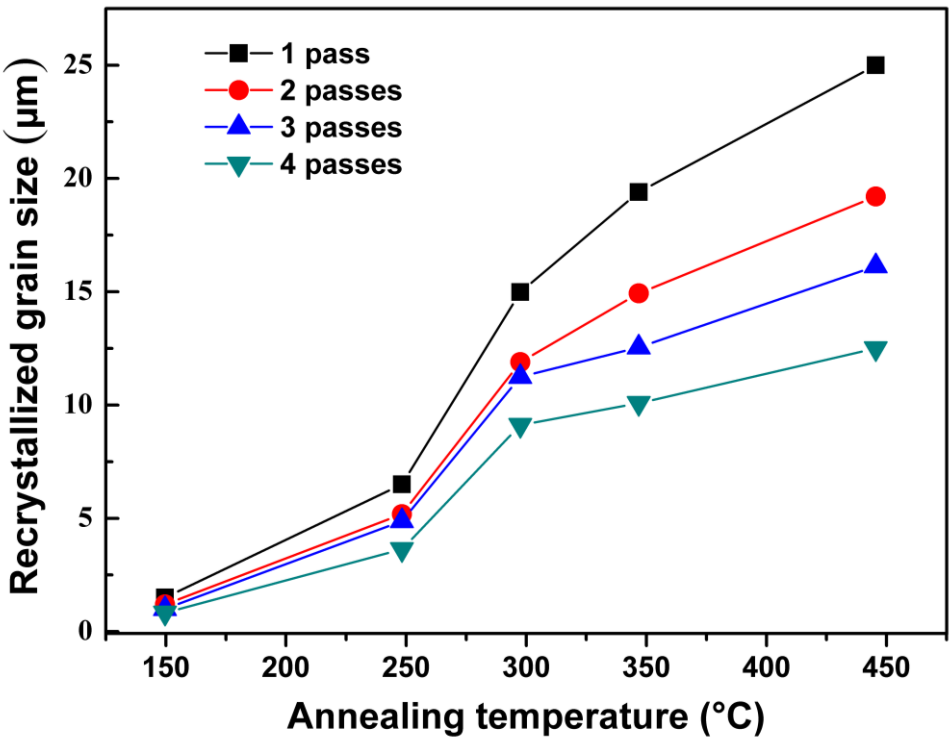

Figure 6

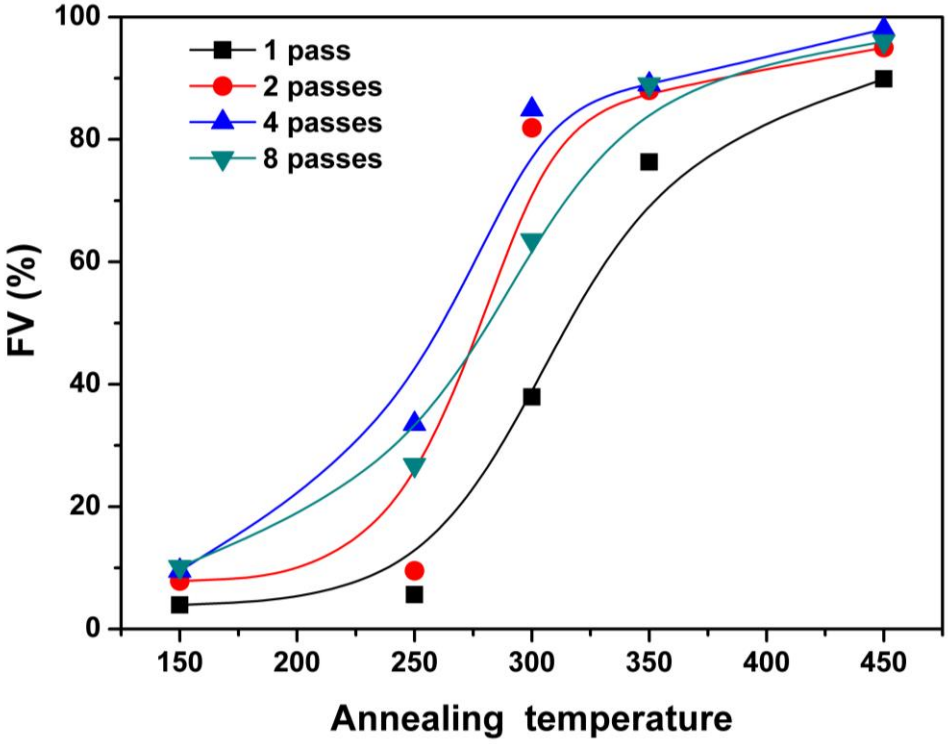

Figure 7

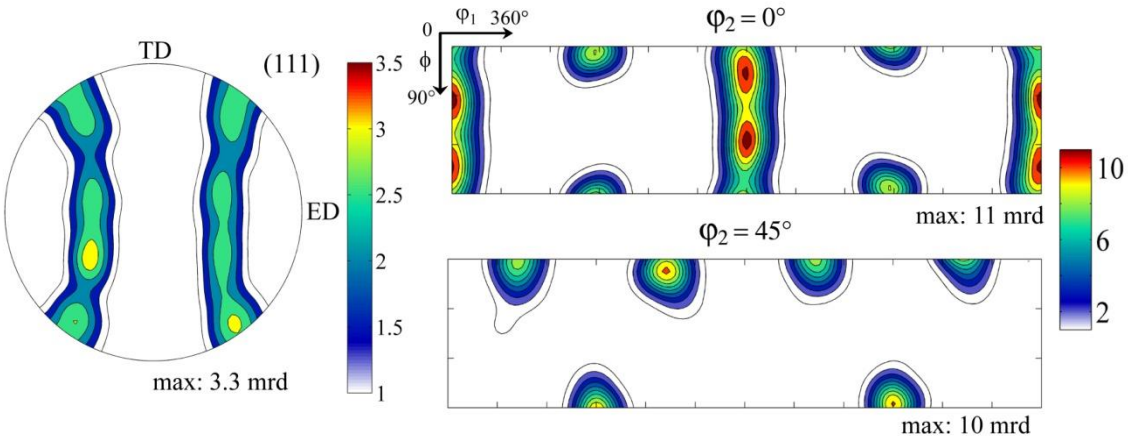

Figure 8

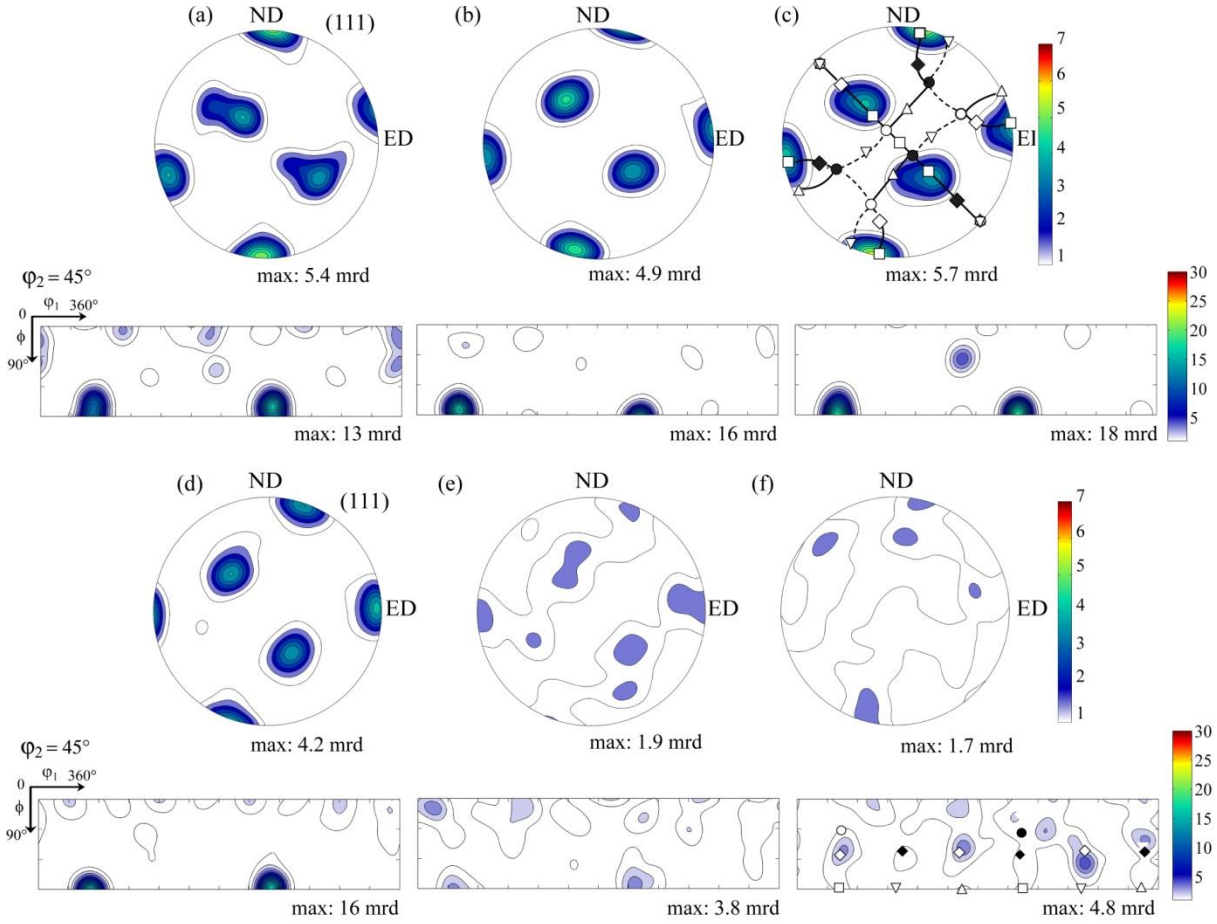
(a)
ND
(111)
ED
max: 5.4 mrd
(b)
ND
ED
max: 4.9 mrd
(c)
ND
ED
max: 5.7 mrd
7
6
5
4
3
2
1
φ2 = 45°
φ1 360°
0
ϕ
90°
max: 13 mrd
max: 16 mrd
max: 18 mrd
30
25
20
15
10
5
(d)
ND
(111)
ED
max: 4.2 mrd
(e)
ND
ED
max: 1.9 mrd
(f)
ND
ED
max: 1.7 mrd
7
6
5
4
3
2
1
φ2 = 45°
φ1 360°
0
ϕ
90°
max: 16 mrd
max: 3.8 mrd
max: 4.8 mrd
30
25
20
15
10
5

Figure 9

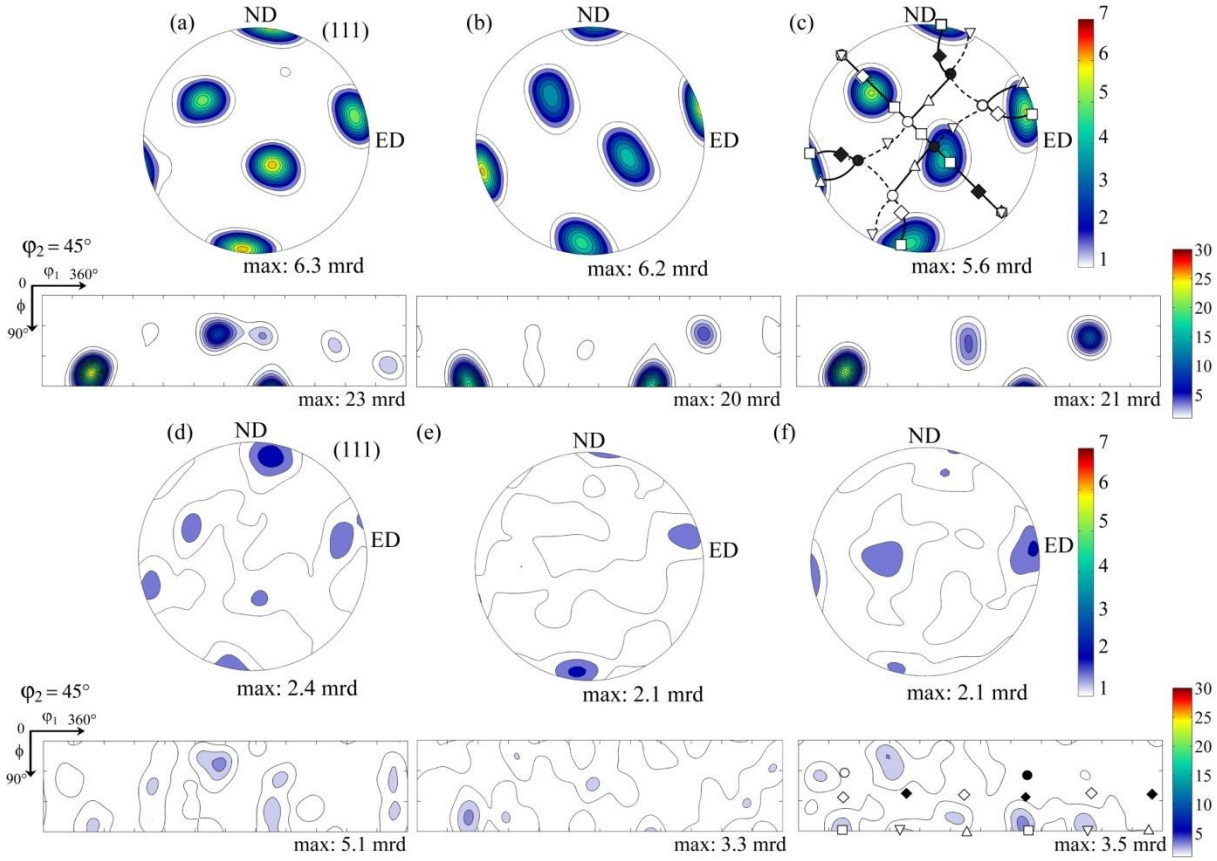
(a)
ND
(111)
ED
max: 6.3 mrd
(b)
ND
ED
max: 6.2 mrd
(c)
ND
ED
max: 5.6 mrd
7
6
5
4
3
2
1
φ2 = 45°
φ1 360°
0
ϕ
90°
max: 23 mrd
max: 20 mrd
max: 21 mrd
30
25
20
15
10
5
(d)
ND
(111)
ED
max: 2.4 mrd
(e)
ND
ED
max: 2.1 mrd
(f)
ND
ED
max: 2.1 mrd
7
6
5
4
3
2
1
φ2 = 45°
φ1 360°
0
ϕ
90°
max: 5.1 mrd
max: 3.3 mrd
max: 3.5 mrd
30
25
20
15
10
5

Figure 10

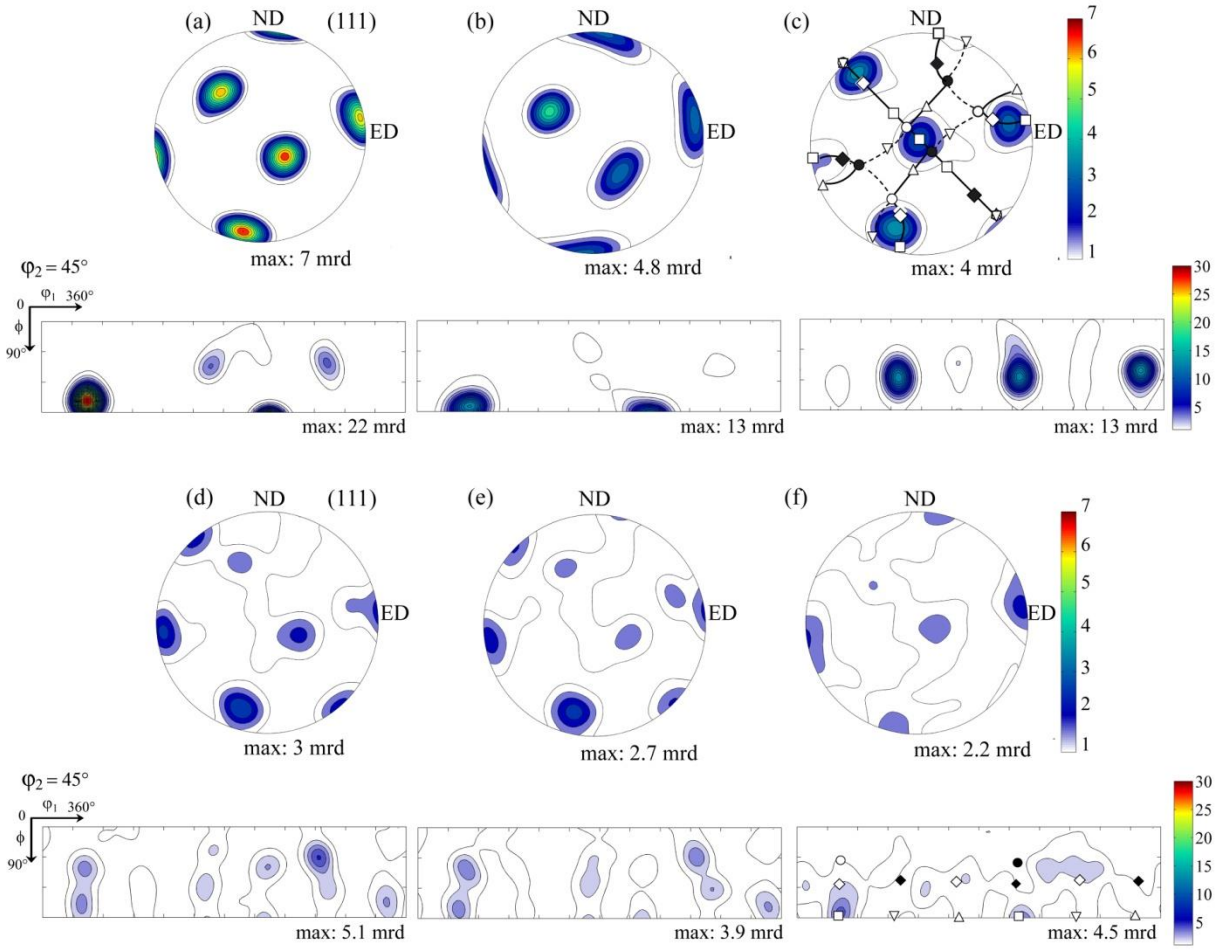
(a)
ND
(111)
ED
max: 7 mrd
(b)
ND
ED
max: 4.8 mrd
(c)
ND
ED
max: 4 mrd
7
6
5
4
3
2
1
φ2 = 45°
φ1 360°
0
ϕ
90°
max: 22 mrd
max: 13 mrd
max: 13 mrd
30
25
20
15
10
5
(d)
ND
(111)
ED
max: 3 mrd
(e)
ND
ED
max: 2.7 mrd
(f)
ND
ED
max: 2.2 mrd
7
6
5
4
3
2
1
φ2 = 45°
φ1 360°
0
ϕ
90°
max: 5.1 mrd
max: 3.9 mrd
max: 4.5 mrd
30
25
20
15
10
5

Figure 11

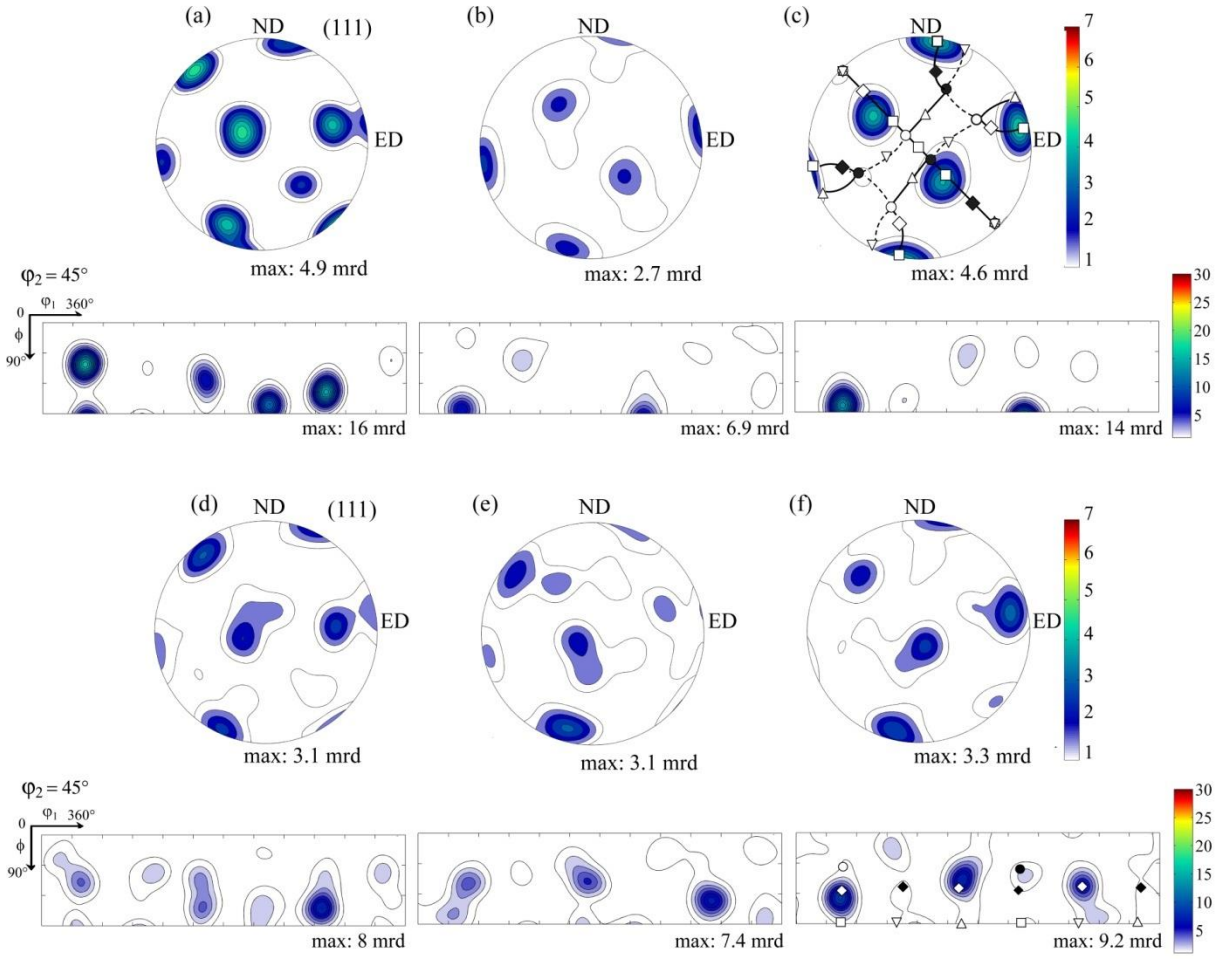
(a)
ND
(111)
ED
max: 4.9 mrd
(b)
ND
ED
max: 2.7 mrd
(c)
ND
ED
max: 4.6 mrd
7
6
5
4
3
2
1
φ2 = 45°
φ1 360°
0
ϕ
90°
max: 16 mrd
max: 6.9 mrd
max: 14 mrd
30
25
20
15
10
5
(d)
ND
(111)
ED
max: 3.1 mrd
(e)
ND
ED
max: 3.1 mrd
(f)
ND
ED
max: 3.3 mrd
7
6
5
4
3
2
1
φ2 = 45°
φ1 360°
0
ϕ
90°
max: 8 mrd
max: 7.4 mrd
max: 9.2 mrd
30
25
20
15
10
5

Figure 12

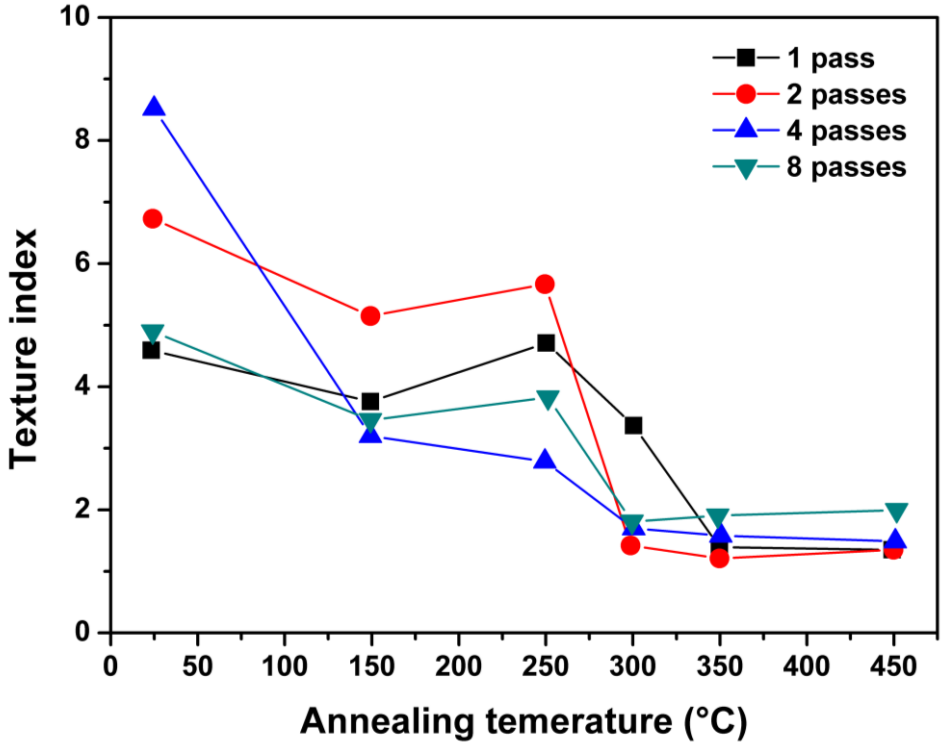

Figure 13

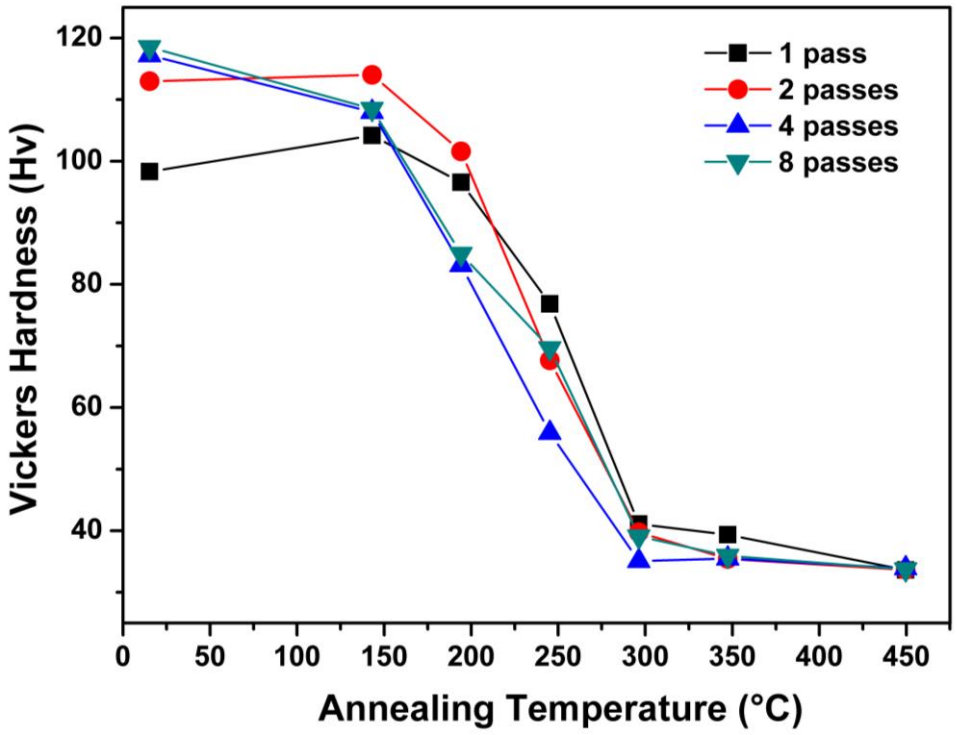

Figure 14

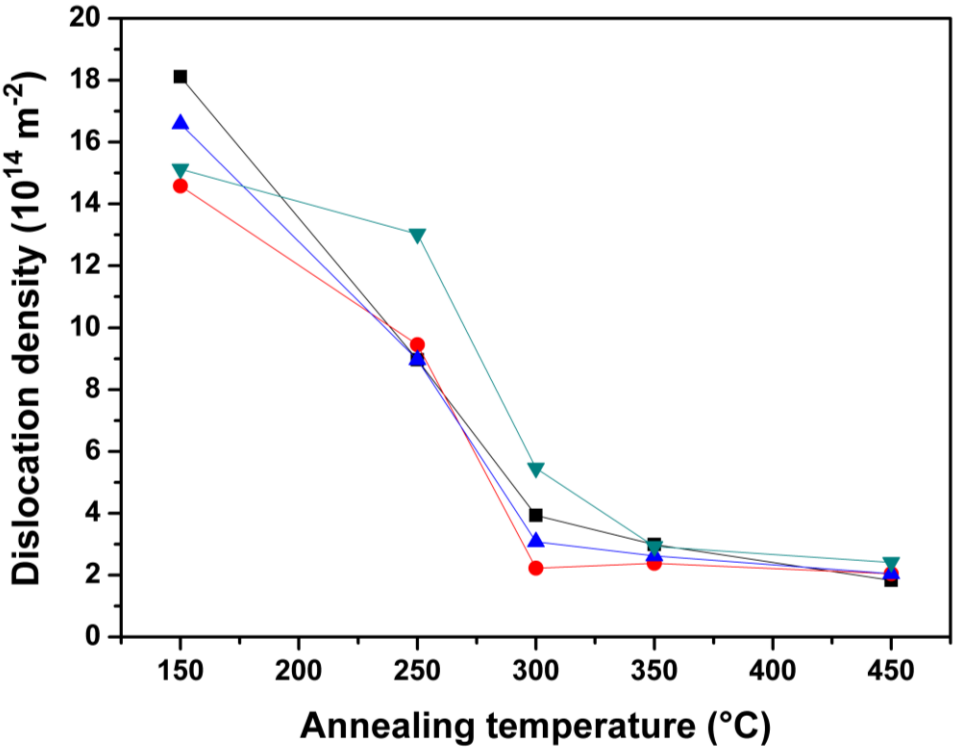
Dislocation density (10^{14} m^{-2})
0
2
4
6
8
10
12
14
16
18
20
150
200
250
300
350
400
450
Annealing temperature (°C)

Figure 15

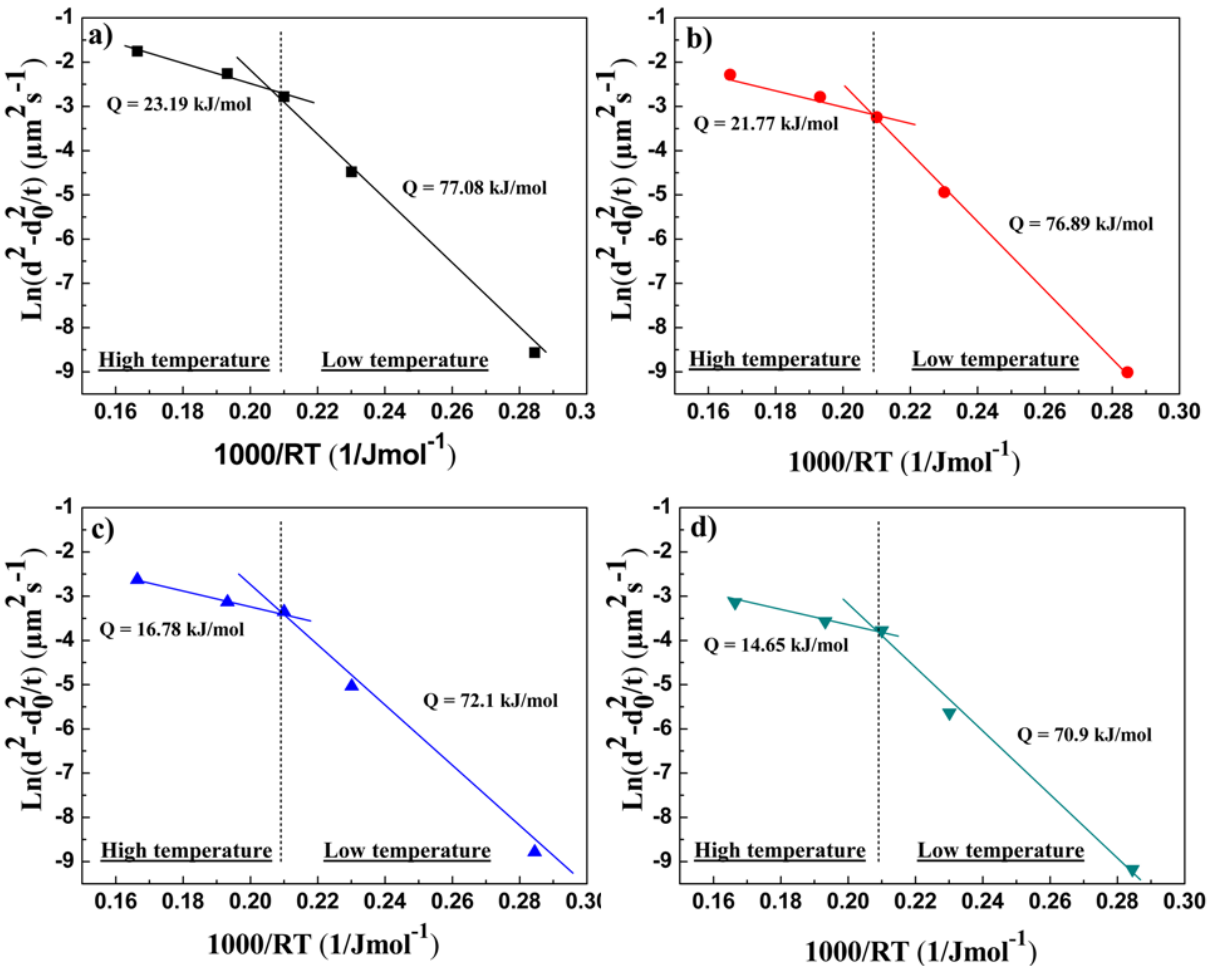

Figure 16

Table 1

Notation		Euler angles (°)		
		φ_1	ϕ	φ_2
△	A_1^*	170.26/ 350.26	90	45
▽	A_2^*	99.74/279.74	90	45
○	A	45	35.26	45
●	$\overline{A}$	225	35.26	45
◇	B	45/165/285	54.74	45
◆	$\overline{B}$	105/225//345	54.74	45
□	C	45/225	90	0